Taylor & Francis
Taylor & Francis Group

In pursuit of natural occurring chiral dienes {(R/S)-carvone} as bidentate ligands for coordination to rhodium(I)

Zaskia Bezuidenhout and Andreas Roodt

Department of Chemistry, University of the Free State, Bloemfontein, South Africa

ABSTRACT

Bis-rhodium-*mu*-chlorido dinuclear complexes with natural occurring limonene-type enantiomeric diene nucleophiles, (S)- and (R)-carvone [**S**Car and **R**Car], are presented and their single crystal structures reported. Utilizing the diolefinic bonds of the carvones, *mu*-[Rh^I(**S**Car)Cl]$_2$ (**IA/B**) and *mu*-[Rh^I(**R**Car)Cl]$_2$ (**IIA/B**) were obtained in ca. 80% yields in clean reactions with reactant RhCl$_3$(H$_2$O)$_x$. The "structured" chiral nanomaterials (**IA/B** and **IIA/***B* > 1.1 nm) crystallize as two independent, dinuclear chiral molecules *Syn-mu*-[Rh^I(**S**Car)Cl]$_2$ (**IA**), *Anti-mu*-[Rh^I(**S**Car)Cl]$_2$ (**IB**), and *Syn-mu*-[Rh^I(**R**Car)Cl]$_2$ (**IIA**, *Anti-mu*-[Rh^I(**R**Car)Cl]$_2$ (**IIB**), respectively (based on the relative orientation of the carvone ring, oxo and methyl groups). Principal differences between the **IA/IIA** *vs* **IB/IIB** complexes in the solid state include the relative orientation of the two carvones, inducing a significant distortion in the μ^2-Rh$_2$Cl$_2$ core, with the dihedral angles of 49.7(1)°/49.73(6)° in **IA/IIA** (*Syn-mu* geometry), versus 23.8(1)°/24.00(6)° in **IB/IIB** (*Anti-mu* geometry), respectively. The presence of the two structurally independent complexes in the solid state is also inferred from ^{1}H NMR spectra.

CONTACT Andreas Roodt ✉ aroodta@gmail.com ⬚ Department of Chemistry, University of the Free State, Box 339, Bloemfontein 9300, South Africa
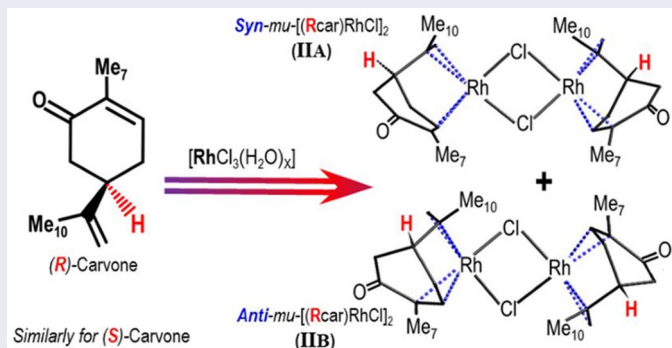Dedicated to Professor Jim D. Atwood on completing his extended term as editor, *Journal of Coordination Chemistry*.
⊕ Supplemental data for this article can be accessed online at https://doi.org/10.1080/00958972.2024.2448520.

GRAPHICAL ABSTRACT

Exploiting the diolefinic bonds of (**R/S**)-carvone in the reaction with RhCl₃(H₂O)ₓ enabled the high-yield synthesis and SCXRD of the "structured" dinuclear enantiomeric nanomaterials *Syn-mu*-[Rhᴵ(**R**Car)Cl]₂ (**IIA**) and *Anti-mu*-[Rhᴵ(**R**Car)Cl]₂ (**IIB**).

1. Introduction

Traditional herbal preparations that play an important role in African culture have over the years been successful for producing potential drug leads [1–3]. The affordability and relatively lower costs of plant preparations are incentives to consider natural product medicines as alternatives to synthetic drugs [4], and are preferred by many indigenous people [5]. Formulations derived from these medicinal plants are utilized across the world and have resulted in several patents [6], and more governments encourage allopathic medicine practitioners to collaborate with traditional medicine practitioners to also allow people access to healthcare [7,8].

The antibacterial effects of limonene-type natural-occurring dienes present in an essential oil found in the pericarp of *Citrus sinensis* suggest it as a possible candidate for developing chemotherapeutic agents against infection from bacterial pathogens [9], since these extracts contain biologically active terpenoids which promotes antimicrobial activities [10]. Limonene along with amounts of carveol and (R)–carvone, is also found in the essential oil of *Lippia scaberrima*, a popular health tea in South Africa, showing hepatoprotective- and antimycobacterial activity. Similarly, essential oils of *Lippia alba* [11] contain monoterpenes like myrcene, limonene and carvone, exhibiting antiviral, antifungal, anti–inflammatory and antibacterial activity. The antitumor and cytotoxic effects of extracts from *L. alba* and main components of citral and carvone chemotypes in its essential oils have been established but the activities in various chemotypes received little attention [12].

Carvone, like limonene, is a diolefinic monoterpene which exists naturally as two enantiomers: (R)-carvone [(–)-carvone; L-carvone] and (S)-carvone [(+)-carvone; D-carvone], (Figure 1), used as starting materials for synthesizing complex terpenoids. Both enantiomers have well-recognized flavors and aromas, with (R)-carvone the dominant
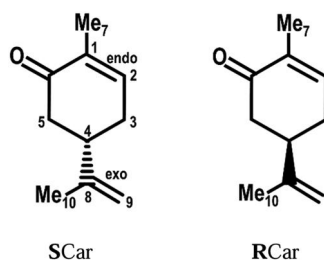
Figure 1. Structures of the carvone diene ligands {including the NMR numbering system used} (S)-Carvone (**S**Car) and (R)-Carvone (**R**Car). Note that although the numbering within the individual complexes follows this general nomenclature, suffixes A–D were added to distinguish between different isomers.

compound in spearmint oil, while (S)-carvone is a key component in caraway and dill seed essential oils. The world market for (R)-carvone (3800 t/year), is much larger than that of the (S)-isomer (10 t/year). About half is synthesized from (R)-limonene, while an estimated 50% is extracted from natural mint [13].

Biological activity studies on carvone indicated its potential use as an adjunct host–directed therapy for tuberculosis [9]. (R)–carvone has also been tested against breast cancer cell lines and displayed substantial toxicity and was explored for apoptotic ability within these cell lines [9]. Attaching carvone to metal centers such as platinum or platinum group elements (PGEs), with known chemotherapeutical properties, may in principle allow manipulation of the activity of the specific compound(s) in a selective and ordered way.

One possibility is to utilize the diene coordinating nature of carvone. Metal alkene complexes are intermediates in many important catalytic reactions and olefins display especially stable bonding in d [8] square planar complexes of Rh^I, Ir^I, Pd^{II}, and Pt^{II} [14]. Rhodium–olefin complexes are e.g. often intermediate species in rhodium–catalyzed olefin hydrogenation reactions [15] and olefin–to–olefin addition reactions [16–18]. When reacting a diene with PGE salts, the diene may form a chelated complex with only one metal atom, such as e.g. with (R/S)–Limonene [19,20], in which the diolefin is strained and different conformations are possible.

Complexes of the type [(diene)RhCl]$_2$ are generally prepared by the reaction of hydrated Rh(III) chloride with the diolefin, and have been established with cyclooctadiene (cod), cyclooctene, cycloheptene, 1,5–hexadiene and 1,3–cyclohexadiene [21]. μ–Dichlorido-bis(cyclooctadiene)dirhodium(I) was prepared by Chatt and Venanzi [22] by refluxing an ethanolic solution of $RhCl_3$ and cyclooctadiene, or by using sodium borohydride as reductant [23], or by the displacement of coordinated ethylene in [(C$_2$H$_4$)$_2$RhCl]$_2$ by cyclooctadiene [24,25].

Using the concept employed by SASOL and others in the early 2000s to prepare funtionalized tertiary phosphine ligands for hydroformylation reactions [26–31], we synthesized the title complexes containing (R/S)-carvone successfully and present here a detailed account of our experiments. We also report the serendipitous but fascinating discovery of different solution and solid-state induced isomers of these structured chiral nanomaterials
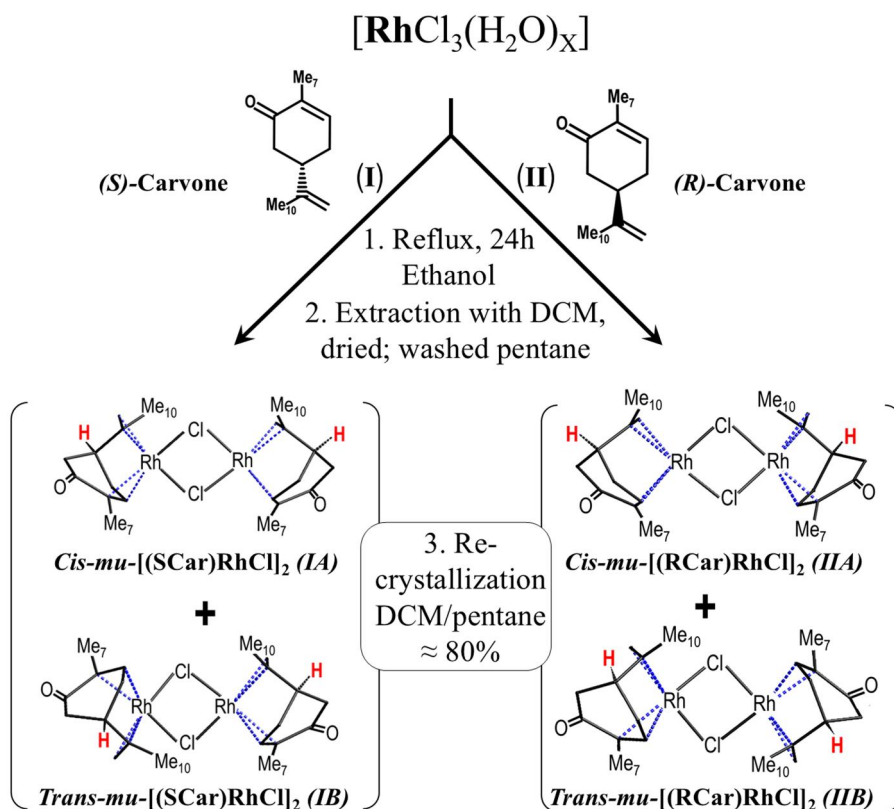
$$[\mathbf{RhCl}_3(H_2O)_X]$$

Figure 2. The general reaction scheme for the preparation of different *mu*-[Rh(*LL'*)Cl]$_2$ complexes (*LL'* = **R**Sar, **R**Car), (**IA/B** and **IIA/B**) illustrating the formation of both the *Syn-mu*- (**IA** and **IIA**) and *Anti-mu*-entities (**IB** and **IIB**); as defined by the relative position of the carvone ring, oxo- and methyl groups.

2. Experimental

2.1. General procedures and instrumentation

All reagents used in the synthesis procedures (Figure 2) were analytical grade chemicals purchased from Sigma–Aldrich and were used, unless stated otherwise, without further purification. All synthesized complexes were characterized by elemental analyses from Atlantic Microlab, Inc., Norcross, Georgia, USA. The infrared spectra from neat samples were recorded using the ATR sampling technique on a Thermo Scientific Nicolet iS10 FT–IR spectrophotometer with a laser range of 4000–400 cm^{-1} and are reported in cm^{-1}. A Varian Cary 50 Conc spectrophotometer was used to collect UV/Vis spectra with 1.000 ± 0.001 cm path length tandem quartz cells. The spectrophotometer unit was equipped with a Thermo Scientific temperature control water bath (accuracy of ± 0.1 °C) fitted with a circulator. The ^{1}H and ^{13}C NMR spectra for all the ligands and rhodium(I) complexes were recorded on a Bruker Avance II 600 (^{1}H: 600 MHz, ^{13}C: 151 MHz). The chemical shifts (δ) are relative to tetramethylsilane (TMS) and are reported in ppm, with both ^{1}H and ^{13}C NMR spectra referenced internally using residual protons in the corresponding deuterated solvent (CDCl$_3$: s, 7.26 ppm

and t, 77.23 ppm, respectively). Crystals suitable for X–ray diffraction were obtained as described in Par. 2.2. All diffraction data were collected on a Bruker APEX–II CCD diffractometer at 100 K using monochromatic Mo Kα radiation (0.71073 Å). Multi–scan absorption corrections were made using SADABS–2016/2 [32] where the cell parameters were refined by SAINT V8.38A [33]. Structures were solved using intrinsic phasing in SHELXT 2018/3 [34] and refined by full matrix least squares against F^2 with all reflections using SHELXL 2018/3 [34] within Olex2 1.3 [35]. Anisotropic displacement parameters were used for all non–hydrogen atoms. The molecular graphics were done using DIAMOND [36] and structural overlays were illustrated using Mercury [37], which was also used to calculate RMS values.

2.2. Synthesis and characterization of complexes

2.2.1. Spectroscopic characterization of the dienes
The ^1H and ^{13}C NMR spectra for the carvone diolefins (Figure 1) as purchased and used in this study are provided below for comparison purposes [38]. The shielding effect of the coordinated ligands by the Rh(I) could also be noted. Direct comparison of the NMR chemical shifts of the signals of the ligands with the relevant Rh(I) complexes (Figure 3) verified the coordination of the ligands to the applicable metal center.
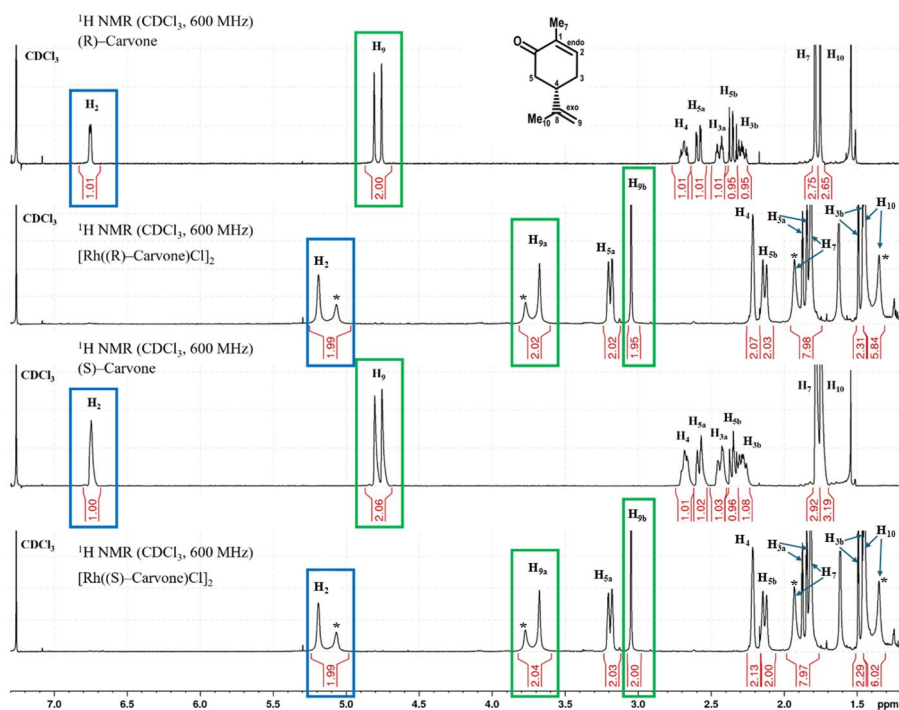
Figure 3. Stacked ^1H NMR spectra of **S**Car, *mu*-[Rh(**S**Car)Cl]$_2$, **R**Car and *mu*-[Rh(**R**Car)Cl]$_2$ in CDCl$_3$. Also indicated are the assumed isomeric components of the *Syn* and the *Anti* distribution as illustrated by the XRD. The numbering of the ligands (Figure 1) stays consistent in both complexes.

2.2.1.1. (S)-carvone (SCar) (I). ^{1}H NMR (CDCl$_3$, 600 MHz): δ 6.74–6.76 (m, 1H, H$_2$), 4.78 (d, 2H,[2]J (H$_{9b}$–H$_{9a}$) = 30.1 Hz, H$_9$), 2.66–2.71 (m, 1H, H$_4$), 2.58 (dd, 1H, [2]J (H$_{5b}$–H$_{5a}$) = 16.0 Hz, [3]J (H$_4$–H$_{5a}$) = 3.6 Hz, H$_{5a}$), 2.42–2.46 (m, 1H, H$_{3a}$), 2.35 (dd, 1H, [2]J (H$_{5a}$–H$_{5b}$) = 16 Hz, [3]J (H$_4$–H$_{5b}$) = 13.4 Hz, H$_{5b}$), 2.26–2.31 (m, 1H, H$_{3b}$), 1.78–1.79 (m, 3H, H$_7$), 1.75 (s, 3H, H$_{10}$).

^{13}C NMR (CDCl$_3$, 151 MHz): δ 200.4 (s, 1 C, C$_6$), 146.9 (s, 1 C, C$_8$), 144.8 (s, 1 C, C$_2$), 135.7 (s, 1 C, C$_1$), 110.7 (s, 1 C, C$_9$), 43.4 (s, 1 C, C$_5$), 42.7 (s, 1 C, C$_4$), 31.5 (s, 1 C, C$_3$), 20.7 (s, 1 C, C$_{10}$), 15.9 (s, 1 C, C$_7$).

2.2.1.2. (R)-carvone (RCar) (II). ^{1}H NMR (CDCl$_3$, 600 MHz): δ 6.74–6.76 (m, 1H, H$_2$), 4.78 (d, 2H, [2]J (H$_{9b}$–H$_{9a}$) = 30.1 Hz, H$_9$), 2.66–2.71 (m, 1H, H$_4$), 2.58 (ddd, 1H, [2]J (H$_{5b}$–H$_{5a}$) = 16.0 Hz, [3]J (H$_4$–H$_{5a}$) = 3.7 Hz, [4]J (H$_{3a}$–H$_{5a}$) = 1.5 Hz, H$_{5a}$), 2.42–2.46 (m, 1H, H$_{3a}$), 2.35 (dd, 1H, [2]J (H$_{5a}$–H$_{5b}$) = 16 Hz, [3]J (H$_4$–H$_{5b}$) = 13.4 Hz, H$_{5b}$), 2.26–2.31 (m, 1H, H$_{3b}$), 1.78–1.79 (m, 3H, H$_7$), 1.75 (s, 3H, H$_{10}$).

^{13}C NMR (CDCl$_3$, 151 MHz): δ 200.4 (s, 1 C, C$_6$), 146.9 (s, 1 C, C$_8$), 144.8 (s, 1 C, C$_2$), 135.7 (s, 1 C, C$_1$), 110.7 (s, 1 C, C$_9$), 43.4 (s, 1 C, C$_5$), 42.7 (s, 1 C, C$_4$), 31.5 (s, 1 C, C$_3$), 20.7 (s, 1 C, C$_{10}$), 15.9 (s, 1 C, C$_7$).

2.2.2. Synthesis of mu-[Rh(LL')Cl]$_2$; (LL'=RCar or SCar)

The different rhodium(I) complexes were prepared by the same general method (Figure 2). The starting material, RhCl$_3$(H$_2$O)$_x$ (500 mg, 1.90 mmol) was dissolved in ethanol (10 mL) and the appropriate diene (2 eq.) was added to the reaction mixture which was left to stir under reflux for 24h. The product was extracted with DCM, dried and washed with pentane. Crystals suitable for SC–XRD analysis were obtained after one week by recrystallization from a mixture of DCM and pentane.

2.2.2.1. Mu-[Rh(SCar)Cl]$_2$.(IA/B). **S**Car (594 μL, 3.80 mmol) was added to RhCl$_3$·3H$_2$O (500 mg, 1.90 mmol) in ethanol to yield bis(S)-carvone-di–μ–chloridodirhodium(I) (496.4 mg, 81.3%).

Anal. Calcd for Rh$_2$C$_{20}$H$_{28}$O$_2$Cl$_2$: C, 41.62; H, 4.89. Found: C, 40.13; H, 4.79.

$$IR \left(cm^{-1}\right) : \nu_{(C=O)} = 1505$$

^{1}H NMR (CDCl$_3$, 600 MHz): δ 5.11 (d, 2H, [2]J ([103]Rh–[1]H) = 74.0 Hz, H$_2$), 3.70 (d, 2H, [2]J ([103]Rh–[1]H) = 57.2 Hz, H$_{9a}$), 3.17 (dd, 2H, [2]J (H$_{3b}$–H$_{3a}$) = 15.3 Hz, [2]J (H$_4$–H$_{3b}$) = 1.6 Hz, H$_{3a}$), 3.03 (s, 2H, H$_{9b}$), 2.19 (s, 2H, H$_4$), 2.11 (d, 2H, [2]J (H$_{3a}$–H$_{3b}$) = 15.3 Hz, H$_{3a}$), 1.85 (d, 6H, [3]J ([103]Rh–[1]H) = 67.7 Hz, H$_7$), 1.84 (dt, 2H, [2]J (H$_{5b}$–H$_{5a}$) = 18.1 Hz, [3]J (H$_4$–H$_{5a}$) = 2.5 Hz, H$_{5a}$), 1.46 (dd, 2H, [2]J (H$_{5b}$–H$_{5a}$) = 18.1 Hz, [3]J (H$_4$–H$_{5b}$) = 3.1 Hz, H$_{5b}$), 1.38 (d, 6H, [3]J ([103]Rh–[1]H) = 58.8 Hz, H$_{10}$).

^{13}C NMR (CDCl$_3$, 151 MHz): δ 205.1 (s, 1 C, C$_6$), 82.9 (s, 1 C, C$_1$), 59.7, (s, 1 C, C$_9$) 41.7 (s, 1 C, C$_5$), 40.2 (s, 1 C, C$_4$), 36.2 (s, 1 C, C$_3$), 26.6 (s, 1 C, C$_{10}$), 20.1 (s, 1 C, C$_7$).

2.2.2.2. Mu-[Rh(RCar)Cl]$_2$. (IIA/B). **R**Car (594 μL, 3.80 mmol) was added to RhCl$_3$·3H$_2$O (500 mg, 1.90 mmol) in ethanol to yield bis(R)-carvone-di–μ–chloridodirhodium(I) (485.4 mg, 79.5%).

Anal. Calcd for $Rh_2C_{20}H_{28}O_2Cl_2$: C, 41.62; H, 4.89. Found: C, 40.23; H, 4.84.

$$IR\ (cm^{-1}):\ \bar{\upsilon}_{(C=C)} =\ 1505$$

^{1}H NMR (CDCl₃, 600 MHz): δ 5.11 (d, 2H, ^2J (^{103}Rh–^{1}H) = 74.0 Hz, H₂), 3.70 (d, 2H, ^2J (^{103}Rh–^{1}H) = 57.2 Hz, H₉ₐ), 3.17 (dd, 2H, ^2J (H₃ᵦ–H₃ₐ) = 15.3 Hz, ^2J (H₄–H₃ᵦ) = 1.6 Hz, H₃ₐ), 3.03 (s, 2H, H₉ᵦ), 2.19 (s, 2H, H₄), 2.11 (d, 2H, ^2J (H₃ₐ–H₃ᵦ) = 15.3 Hz, H₃ₐ), 1.85 (d, 6H, ^3J (^{103}Rh–^{1}H) = 67.7 Hz, H₇), 1.84 (dt, 2H, ^2J (H₅ᵦ–H₅ₐ) = 18.1 Hz, ^3J (H₄–H₅ₐ) = 2.5 Hz, H₅ₐ), 1.46 (dd, 2H, ^2J (H₅ᵦ–H₅ₐ) = 18.1 Hz, ^3J (H₄–H₅ᵦ) = 3.1 Hz, H₅ᵦ), 1.38 (d, 6H, ^3J (^{103}Rh–^{1}H) = 58.8 Hz, H₁₀).

^{13}C NMR (CDCl₃, 151 MHz): δ 205.1 (s, 1 C, C₆), 83.0 (s, 1 C, C₁), 59.8, (s, 1 C, C₉) 41.9 (s, 1 C, C₅), 40.4 (s, 1 C, C₄), 36.3 (s, 1 C, C₃), 26.8 (s, 1 C, C₁₀), 20.3 (s, 1 C, C₇).

3. Results and discussion

3.1. Synthesis of Rh(I) complexes

Dinuclear rhodium(I) complexes of the type [Rh(*LL*′)Cl]₂ (*LL*′ = **R**Car, **S**Car) were successfully synthesized as chlorido–bridged structures containing chelated dienes using the method [22,23] to synthesize [Rh(cod)Cl]₂. However, significantly longer reaction times were required due to the formation of slightly distorted metal–olefin bonds for the more sterically strained carvone diene ligands (Figure 2). Procedures [22] that exclude water gave lower yields since the Rh(III) starting material is only sparingly soluble in ethanol. The addition of sodium carbonate, although shortening the reaction time, results in lower quality products containing impurities whereas increasing the reaction time resulted in better yields [39]. Despite the synthetic difficulties associated with the enantiopure compounds, both complexes **IA/B** and **IIA/B** could be successfully recrystallized from a mixture of DCM and pentane. The yellow plate–like crystals of *mu*-[Rh(**S**Car)Cl]₂ and *mu*-[Rh(**R**Car)Cl]₂ were successfully isolated and analyzed.

3.2. Spectroscopy

The coordination of carvone to Rh(I) is evident from a decrease in the IR stretching frequencies of the olefinic bonds 1505 cm⁻¹ (**IA/B** and **IIA/B**). The $\nu_{(C=O)}$ absorption band remains unchanged in all the carvone complexes suggesting that the carbonyl group is not involved in the chelate bonding.

Moreover, successful coordination of the carvone dienes to the respective Rh(I) centers was also confirmed by ^{1}H NMR. The ^{1}H NMR signals of both rhodium(I) compounds, **IA/B** and **IIA/B**, do not display the expected prominent coupling to the 100% natural abundant [103]Rh nucleus (see Figure 3), assumed to be due to fast exchange kinetics within these complex molecules. However, non-equivalent splitting of olefinic protons and both the methyl groups (asterisked peaks in Figure 3; *ca.* in a 1:2 ratio) indicates that the two different isomers (*Syn* and *Anti*) exist in solution already, albeit exhibiting very fast dynamic interchange, known for Rh(I) and PGE elements [40–42].
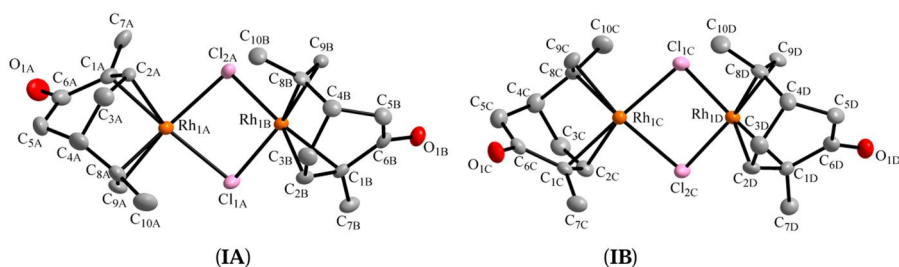
Figure 4. Molecular representation and numbering of *mu*-[Rh(**S**Car)Cl]$_2$ (**IA/B**) viewed along the *b*-axis. The displacement ellipsoids are drawn at 50% probability level with hydrogen atoms excluded for clarity. The four metal centers and carvone ligands are numbered the same with the addition of the suffixes A–D, respectively for each. **IA** = *Syn-mu*-[Rh(**S**Car)Cl]$_2$ and **IB** = *Anti-mu*-[Rh(**S**Car)Cl]$_2$; based on the relative orientation of the carvone ring (Rh-C9-olefinic bonds), oxo- and methyl groups.
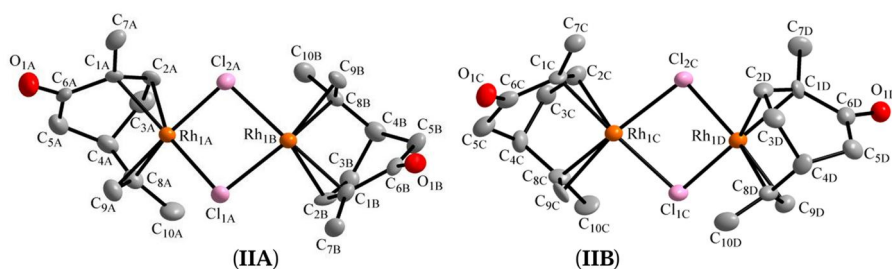

Figure 5. Molecular representation and numbering scheme of *mu*-[Rh(**R**Car)Cl]$_2$ (**IIA/B**) viewed along the *b*-axis. The displacement ellipsoids are drawn at 50% probability level with hydrogen atoms excluded for clarity. The four metal centers and carvone ligands are numbered the same with the addition of the suffix A–D, respectively for each. **IIA** = *Syn-mu*-[Rh(**R**Car)Cl]$_2$ and **IIB** = *Anti-mu*-[Rh(**R**Car)Cl]$_2$; based on the relative orientation of the carvone ring (Rh-C9-olefinic bonds), oxo- and methyl groups.

3.3. X-ray crystallography

A thorough search was conducted on the Cambridge Structural Database (CSD) [43] for any metal complexes containing the limonene/carvone-type backbones as monodentate or bidentate ligands. Only one applicable rhodium(I) crystal structure was identified which reports the complex, [Rh(**S**Car)Cp] [44] containing **S**Car as a bidentate ligand and cyclopentadienyl as a pentahapto (η^5) ligand, chosen based on the presence of a diolefinic bidentate ligand consisting of a carvone backbone and allows crystallographic comparisons with the complexes reported here. Thus, rhodium syntheses led to the crystallization and collection of *mu*-[Rh(**S**Car)Cl]$_2$ (**IA/B**) (Figure 4) and *mu*-[Rh(**R**Car)Cl]$_2$ (**IIA/B**) (Figure 5). Both the compounds as isolated represent novel examples of carvone acting as bidentate ligand which could be structurally studied.

Crystallographic data, details of data collection and refinement parameters for all the crystal structures are shown in Table 1. Important bond parameters are indicated under each subsequent crystal structure. The hydrogen atoms and numbering of certain carbon atoms were omitted for clarity on some molecular structures. Detailed lists of crystallographic parameters of all the presented structures are given in the supplementary data. Complete lists of bond angles, bond distances, atomic coordinates,

Table 1. Crystallographic data and refinement parameters of mu-[Rh(SCar)Cl]$_2$ (IA/B) and mu-[Rh(RCar)Cl]$_2$ (IIA/B).

Crystallographic data	IA/B	IIA/B
Empirical formula	$C_{20}H_{28}Cl_2O_2Rh_2$	$C_{20}H_{28}Cl_2O_2Rh_2$
Formula weight	577.14	577.14
Temperature (K)	100(2)	100(2)
Crystal system	Orthorhombic	Orthorhombic
Space group	$P2_12_12_1$	$P2_12_12_1$
Unit cell dimensions		
a (Å)	11.8507(6)	11.839(1)
b (Å)	12.1450(7)	12.117(1)
c (Å)	28.184(1)	28.162(3)
α (°)	90	90
β (°)	90	90
γ (°)	90	90
Volume (Å^3)	4056.4(4)	4043.1(6)
Z	8	8
Density (Mg/m^3)	1.890	1.896
Crystal color	Yellow	Yellow
Crystal morphology	Plate	Plate
Crystal size (mm^3)	$0.200 \times 0.189 \times 0.043$	$0.200 \times 0.104 \times 0.041$
μ (mm^{-1})	1.903	1.909
$F(000)$	2304	2304
Θ range (°)	1.83–28.34	1.83–28.36
Index ranges	$-15 \leq h \leq 15$	$-15 \leq h \leq 15$
	$-16 \leq k \leq 16$	$-16 \leq k \leq 15$
	$-37 \leq l \leq 37$	$-37 \leq l \leq 37$
Reflections collected	73,946	50,860
Unique reflections	10,101	10,070
R_{int}	0.0869	0.0846
Completeness to Θ max (%)	99.8	99.8
Data / restraints / parameters	10,101 / 0 / 495	10,070 / 0 / 487
Goodness–of–fit on F^2	1.074	1.146
$R [I > 2\sigma(I)]$	$R_1 = 0.0337$	$R_1 = 0.0596$
	$wR_2 = 0.0611$	$wR_2 = 0.1095$
R (all data)	$R_1 = 0.0444$	$R_1 = 0.0972$
	$wR_2 = 0.0647$	$wR_2 = 0.1313$
ρ_{max}, ρ_{min} (e.Å^{-3})	0.81, −0.99	1.38, −1.49
Flack parameter	−0.02(4)	0.30(8)[a]

[a]Obtained as batch scale factor following refining the data with a TWIN instruction as defined in OLEX [33].

hydrogen atom coordinates, torsion angles and anisotropic displacement parameters of the complexes are available.

3.3.1. Mu-[Rh(SCar)Cl]$_2$ (IA/B)

The dinuclear title compound **IA/B**, bis(S)-Carvone)-di–μ–chloridodirhodium(I) crystallizes in the orthorhombic crystal system in the space group $P2_12_12_1$ with eight formula units in the unit cell ($Z = 8$) and two independent dinuclear entities in the asymmetric unit (Figure 4). The structure showed no statistical disorders and required no restraints. Anomalous dispersion effects in diffraction measurements were used to determine the absolute structure of the non–centrosymmetric space group. The value of the Flack parameter of −0.02(4) indicates that the absolute structure given by the structure refinement is correctly assigned, in agreement with the use of the enantiomeric pure **S**Car ligand for the synthesis. Selected bond lengths, bond-, dihedral-, and torsion angles are given in Table 2.

Note that individual bond parameters in the structures of **IA/B** are next discussed in detail, but those in **IIA/B** (quite similar to that of **IA/B**), although given in Table 2,

Table 2. Selected crystallographic data for mu-[Rh(SCar)Cl]₂ (IA/B), mu-[Rh(RCar)Cl]₂ (IIA/B) and [Rh(SCar)Cp] [44] (E).

Parameter	IA SCar-syn-mu		IB SCar-anti-mu		IIA RCar-syn-mu		IIB RCar-anti-mu		E Cp-Scar
Rh metal centers=	A	B	C	D	A	B	C	D	Cp-Scar
Atoms									
Bond length/ Intra-atomic distance (Å)									
Rh–Cl$_1$	2.396(2)	2.405(2)	2.380(2)	2.389(2)	2.399(4)	2.404(3)	2.378(3)	2.387(4)	–
Rh–Cl$_2$	2.378(2)	2.376(2)	2.393(2)	2.386(2)	2.374(4)	2.377(3)	2.396(4)	2.384(4)	–
Rh–X$_{endo}$	2.0127(5)	2.0234(5)	2.0095(6)	2.0219(5)	2.037(1)	2.016(1)	2.0129(9)	2.019(1)	2.0558(3)
Rh–C$_1$	2.163(6)	2.161(6)	2.155(6)	2.176(6)	2.18(1)	2.14(1)	2.15(1)	2.16(1)	2.21(2)
Rh–C$_2$	2.101(6)	2.123(6)	2.099(6)	2.107(6)	2.13(1)	2.12(1)	2.11(1)	2.12(1)	2.15(2)
Rh–X$_{exo}$	2.0367(6)	2.0230(5)	2.0405(5)	2.0403(6)	2.0415(9)	2.0227(9)	2.052(1)	2.0464(9)	2.0727(4)
Rh–C$_8$	2.174(6)	2.154(6)	2.168(6)	2.178(6)	2.18(1)	2.15(1)	2.18(1)	2.18(1)	2.16(2)
Rh–C$_9$	2.133(6)	2.128(6)	2.140(6)	2.131(6)	2.14(1)	2.13(1)	2.16(1)	2.15(1)	2.21(2)
C$_1$–C$_2$	1.410(8)	1.409(9)	1.399(9)	1.416(9)	1.40(2)	1.38(2)	1.40(2)	1.40(2)	1.45(2)
C$_8$–C$_9$	1.39(1)	1.394(9)	1.384(9)	1.387(9)	1.39(2)	1.41(2)	1.38(2)	1.39(2)	1.39(3)
O–C$_6$	1.224(9)	1.213(7)	1.208(8)	1.239(8)	1.20(2)	1.22(2)	1.22(2)	1.23(2)	1.19(2)
O–O^a	10.83(1)		10.51(1)		10.80(1)		10.40(1)		–
O–H8^a	11.17(1)		12.02(1)		11.16(1)		12.01(1)		–
Bond angle (°)									
Cl$_1$–Rh–Cl$_2$	81.38(5)	81.23(6)	80.96(6)	80.94(6)	81.2(1)	81.1(1)	81.0(1)	81.1(1)	–
Rh–Cl$_1$–Rh^a	86.47(5)		96.29(6)		86.6(1)		96.3(1)		–
Rh–Cl$_2$–Rh^a	87.52(5)		96.01(6)		87.7(1)		95.9(1)		–
Torsion angle (°)									
O–Rh–Rh′–O^a	92.1(4)		131.5(2)		89.9(6)		131.2(3)		–
C9–Rh–Rh′–C9^a	82.5(2)		84.2(2)		82.8(3)		84.7(3)		–
C6–Rh–Rh′–C6^a	175.7(3)		38.7(3)		176.2(6)		37.7(5)		–
Dihedral angle (°)									
$P_{Cl1-Rh-Cl2}$ – $P_{Xendo-Rh-Xexo}$ (τ)^b	6.83(4)	7.95(5)	7.13(5)	4.83(4)	6.76(8)	8.08(9)	6.80(9)	5.20(7)	–
$P_{Rh-C1-C2}$ – $P_{Rh-C8-C9}$ (χ)^c	88.7(3)	87.4(3)	88.0(2)	87.3(3)	88.3(6)	87.3(6)	87.8(5)	87.0(7)	85.6(6)
$P_{Xendo-Xexo-Cl1-Cl2}$ – $P_{Rh-C1-C2}$^{d}	83(1)	85.54(3)	83.9(3)	86.1(3)	83.8(5)	85.0(6)	84.1(7)	86.0(6)	85.2(5)^e
$P_{Xendo-Xexo-Cl1-Cl2}$ – $P_{Rh-C8-C9}$^{d}	69(1)	69.1(3)	69.5(3)	68.3(3)	70.2(7)	69.0(6)	69.0(9)	69.0(2)	65.6(5)^e
$P_{Rh-Cl1-Cl2}$ – $P_{Rh'-Cl1-Cl2}$^{a,f}	49.73(6)		24.00(6)		49.7(1)		23.8(1)		–

^{a}Primed atoms indicate other intra-Rh-fragment.
^{b}Twist angle (τ) of diolefin [45].
^{c}Bite angle of diolefin (χ)[45].
^{d}Coordination plane: $P_{Xendo-Xexo-Cl1-Cl2}$, where X$_{endo}$ and X$_{exo}$ are the midpoints of the two (C$_1$–C$_2$) and (C$_8$–C$_9$) olefinic entities, respectively. ^{e}Coordination plane: $P_{Xendo-Xexo-Cl1-Cl2}$ with X$_{Cp}$ (midpoint of the Cp ring).
^{f}Bent dihedral angle between the two Rh-Cl-Cl′ coordination planes.

are only referred to but not discussed (Par. 3.3.2) yet included in more detail in the Supplementary Material (Par. SII).

The solid–state structure of the compound displays two independent dinuclear molecular entities. Both these complexes each show two rhodium(I) centers connected by two bridging chlorido ligands as well as a peripheral diolefin, **S**Car, which coordinates as a bidentate ligand through its olefinic bonds, to each respective Rh center (denoted by A–D).

The deviation of selected atoms in **IA/B** from the rhodium(I) coordination plane ($\mathbf{P}_{Xendo–Xexo–Cl1–Cl2}$, where X_{endo} and X_{exo} are the midpoints of the two (C_1–C_2) and (C_8–C_9) olefinic entities, respectively), is given in Table S4. Nine formal intramolecular and six formal intermolecular hydrogen bonding interactions were observed and are presented in the Supplementary Material: Table S6 and shown in Figure S5.

The distances from the metal to the individual carbon atoms of the olefinic bonds in **IA/B** (Table 2), which varies from 2.154(6) Å to 2.178(6) Å for C_1 and C_8 and from 2.099(6) Å to 2.140(6) Å for C_2 and C_9, indicates that the olefinic bonds are slightly slanted/rotated with respect to the Rh–X bonds, where C_1 and C_8 are situated further from Rh due to the steric influence of the methyl substituents on both these carbon atoms. This is corroborated by the angles that these olefinic carbon atoms make with the midpoints of each respective double bond and rhodium center, Rh–X_{endo}–C_1 and Rh–X_{exo}–C_8, which ranges between 91.2(5)° and 92.9(5)°.

The different Rh centers exhibit minimal variation in the corresponding bond angles of X_{endo}–Rh–X_{exo}, ranging between 93.33(2)° and 93.87(2)°, or Cl_1–Rh–Cl_2, with values from 80.94(6)° to 81.38(5)°. The X_{endo}–Rh–Cl and X_{exo}–Rh–Cl angles (adjacent $X_{endo/exo}$ and Cl atoms) for Rh_B, Rh_C and Rh_D are all comparable, fluctuating between 92.08(5)° and 92.93(5)°. The carvone coordinated to the Rh_A center has bond angles of 90.44(4)° for X_{endo}–Rh–Cl_{2A}, which is a near ideal square–planar angle, and 94.43(4)° for X_{exo}–Rh–Cl_{1A}, which deviates from the ideal 90° angle. The angles that Rh_A and Rh_B make with a chlorido ligand are 86.47(5)° for Cl_{1A} and 87.52(5)° for Cl_{2A}, whereas the angles that Rh_C and Rh_D make are significantly larger at 96.29(6)° and 96.01(6)° for Cl_{1C} and Cl_{2C}, respectively.

The angles within the carbonyl entity of the carvone ligand are all *ca.* 120°, indicative of the sp^2 nature and corresponding planarity of this entity. A half–chair conformation in the coordinated carvone ligand is the result of all but one carbon atom of the ring (C_4) being in one plane, thus generating two planes, $\mathbf{P}_{C5–C6–C1–C2–C3}$ and $\mathbf{P}_{C3–C4–C5}$, between the principal carvone plane and the chair fragment of the half–chair conformation, varying between 55.0(5)° and 56.5(5)°, respectively. The C_3–C_4–C_5 bond angles range from 107.4(6)° to 108.5(6)° and signifies relief from angle strain, while closely representing the ideal tetrahedral bond angle of 109.5°. The methyl group, C_7, and oxygen are syn–periplanar about the C_1–C_6 bond, therefore contributing to the ring strain, with torsion angles of 8(1)°, 16.2(8)°, 9.2(9)° and 14.1(9)° for $O_{A–D}$, respectively.

The coordination square plane ($\mathbf{P}_{Xendo–Xexo–Cl1–Cl2}$) is defined by the four coordinating ligands of each respective Rh(I) center, where in the case of an olefinic bond, the midpoint of the bond is used. The endocyclic and exocyclic double bonds make angles of 83(1)°–86.1(3)° and 68.3(3)°–69.5(3)°, respectively, with the respective coordination planes. The coordination planes of the two respective metal centers in each
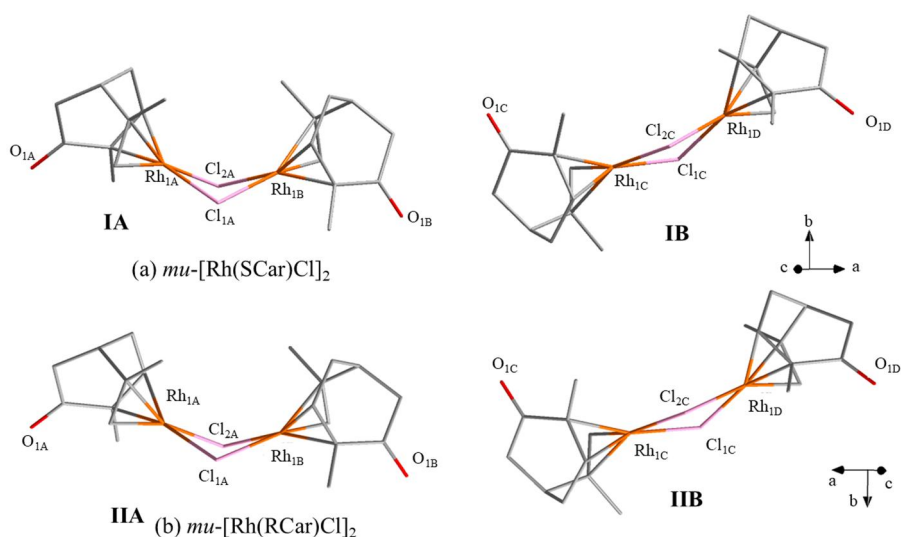
Figure 6. Molecular representation illustrating the difference in bending of the Rh_2Cl_2 core for the two molecules of (a) *mu*-[Rh(**S**Car)Cl]$_2$ (**IA/B**) $\{49.73(6)°\ (Rh_A;Rh_B)$ and $24.00(6)°\ (Rh_C;Rh_D)\}$, and (b) *mu*-[Rh(**R**Car)Cl]$_2$ (**IIA/B**), $\{49.7(1)°\ (Rh_A;Rh_B)$ and $23.8(1)°\ (Rh_C;Rh_D)\}$. Hydrogen atoms and certain atom names are omitted for clarity.

molecule intersect with dihedral angles of 55(1)° and 22.98(2)° for **IA** and **IB**, respectively, resulting in a Rh_2Cl_2 core that is bent by 49.73(6)° ($Rh_A;Rh_B$) and 24.00(6)° ($Rh_C;Rh_D$), respectively (Figure 6). The substantial difference may be attributed to the orientation of the carbonyl groups on the carvone backbone relative to one another and the steric hindrance that accompany this orientation.

Although four carvone ligands have the same basic configuration, the carbonyl oxygen atoms are orientated in opposite directions of the *c*-axis on **IA**, and are positioned in the same direction of the *b*-axis (thus justifying the *Syn* notation, see Figures S6 and S13), whereas the CO-oxygen atoms in **IB** are orientated in the same direction of the *c*-axis positioned but in opposite directions of the *b*-axis (*Anti* notation; Figures S6 and S13). The core therefore bends around the *c*-axis so that the oxygen atoms in **IA** are situated further away from one another. The influence of the orientation of these carbonyl oxygen atoms can also be observed in the $Rh–C_1–C_6–O$ torsion angles, which differ significantly for **IA** with angles of −120.3(7)° for $Rh_A;O_A$ and −109.2(6)° for $Rh_B;O_B$, whereas **IB** has comparable torsion angles of −115.9(6)° for $Rh_C;O_C$ and −114.6(6)° for $Rh_D;O_D$.

The planes through the metal and olefinic carbon atoms of each respective double bond ($\mathbf{P}_{Rh–C1–C2} - \mathbf{P}_{Rh–C8–C9}$) (Figure S9) displays a dihedral angle, denoted as the "bite angle" of the carvone ligand (χ [45]), and varies between 87.3(3)° and 88.7(3)°. The plane through the metal and midpoints of both olefinic bonds is defined by $\mathbf{P}_{Xendo–Rh–Xexo}$ which forms a dihedral angle (twist angles, τ [45]) with the plane through the metal and chlorido ligands, $\mathbf{P}_{Cl1–Rh–Cl2}$. These angles are 6.83(4)°, 7.95(5)°, 7.13(5)° and 4.83(4)° for $Rh_{A–D}$, respectively, indicating that the coordinating ligands about the individual Rh centers are not perfectly planar.

Finally, but probably the most significant 3D differences between **IA** and **IB** are illustrated by the following (Table 2):

- Expanded torsion angles O-Rh-Rh'-O' and C6-Rh-Rh'-C6': 92.1(4)° and 175.7(3)° for **IA**, vs 131.5(2)° and 38.7(3)° for **IB**, justifying the assigned configurations as Syn-mu-[Rh(**S**Car)Cl]$_2$ and Anti-mu-[Rh(**S**Car)Cl]$_2$, respectively (See also the space filling illustrations in the Supplementary Material, Figure S13).
- An almost 10° Rh-Cl1-Rh' and Rh-Cl2-Rh' bond angles which are 86.5(1) and 87.5(1) for **IA**, and 96.3(1)° and (96.0(1)°) in **IB**, respectively.
- More than 25° difference in the dihedral Rh-Cl1-Cl2/Rh-Cl1-Cl2 angles, resulting in a Rh$_2$Cl$_2$ core in **IA** that is bent by 49.73(6)° (Rh$_A$;Rh$_B$), but only by 24.00(6)° (Rh$_C$;Rh$_D$) in **IB**, respectively.
- Total molecule sizes larger than 1 nm (thus structured molecular nano materials), indicated from peripheral O-H8' intra-atomic distances of 11.2(1) Å in **IA**, and 12.0(1) Å and **IB**, respectively. Similarly, the differences in peripheral O-O' intra-atomic distances are 10.83(1) in **IA** and 10.51(1) Å in **IB**, respectively, and are shorter but still significantly different.

3.3.2. Mu-[Rh(RCar)Cl]$_2$ (IIA/B)

The dinuclear title compound **IIA/B**, bis-(R)-Carvone-di-μ-chloridodirhodium(I), was synthesized as described in Par. 2.2. The complex again (as for **IA/B**) crystallizes in the orthorhombic crystal system in the $P2_12_12_1$ space group and has eight formula units in the unit cell ($Z = 8$), with two independent dinuclear entities in the asymmetric unit. **IIA/B** is isomorphous (following inversion) to **IA/B**, with virtually identical cell parameters (Table 1).

The structure showed no statistical disorders and required no restraints. The high electron peak density (1.38 e.Å^{-3}) is located 1.41 Å from Cl$_1$ and the low electron peak density (−1.49 e.Å^{-3}) is located 0.86 Å from the Rh$_2$ atom. Anomalous dispersion effects in diffraction measurements are used to determine the absolute structure of the non–centrosymmetric space group. The value of the Flack parameter of 0.30(8) indicates the presence of a racemic twin, and thus represents the batch scale factor, which was accordingly refined with an appropriate TWIN instruction.

The molecular structure of mu-[Rh(**R**Car)Cl]$_2$ (Figure 5) includes the atomic numbering, with selected bond lengths, bond and dihedral angles given in Table 2. Eight formal intramolecular and five formal intermolecular hydrogen bonding interactions were observed and are presented in the Supplementary Material (Table S11 and Figure S10). The deviation of selected atoms from the Rh(I) coordination plane is given in Table S10.

The solid–state structure of the compound also displays two independent (similar to **IA/B**, Par. 3.3.1), dinuclear molecular entities. Both these complexes each show two rhodium(I) centers connected by two bridging chlorido ligands as well as a diolefin, **R**Car, which coordinates as a bidentate ligand, through its olefinic bonds, to each respective Rh center.

In **IIA** (Rh$_{1A/1B}$), the (R)-carvones are orientated in opposite directions of the c-axis (endo$_{(A)}$ anti to Cl$_{1A}$, endo$_{(B)}$ anti to Cl$_{2A}$), whereas in **IIB** (Rh$_{1C/1D}$), the (R)-carvones are
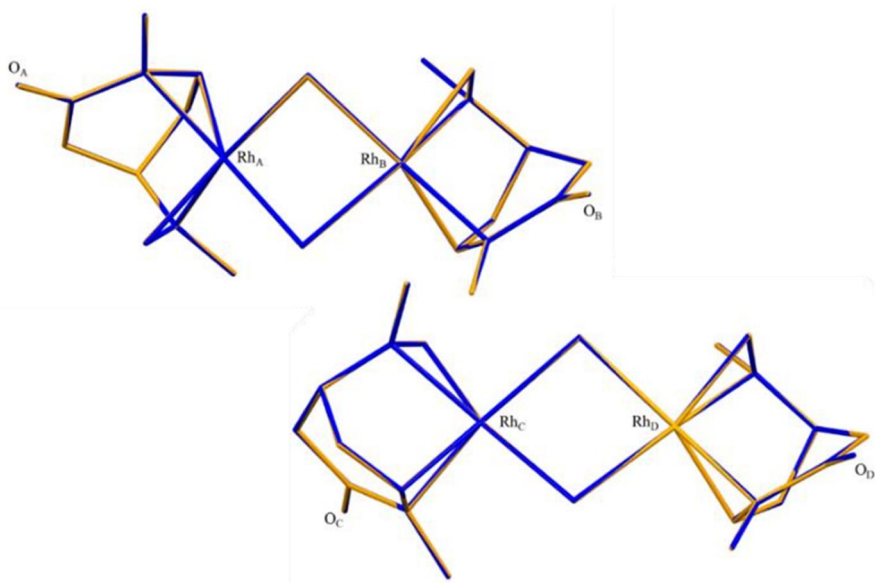
Figure 7. Overlay of the reported structures **IA/B** *mu*-[Rh(**S**Car)Cl]$_2$ (blue) and inverted **IIA/B** *mu*-[Rh(**R**Car)Cl]$_2$ (orange), which gives RMS values of 0.0180 for Rh$_A$;Rh$_B$ and 0.0175 for Rh$_C$;Rh$_D$, respectively.

orientated in the same direction of the *c*-axis (endo$_{(C)}$ and endo$_{(D)}$ *anti* to Cl$_{1C}$). This results in the oxygen atoms of the carbonyl in **IIA** (O$_{1A/1B}$) being positioned in the same direction of the *b*-axis, while the carbonyl oxygen atoms of **IIB** (O$_{1C/1D}$) are positioned in opposite directions of the *b*-axis (see Figures 5 and 6).

As indicated in Par. 3.3.1, since the basic structures of **IA/B** are (apart from being enantiomers) virtually chemically identical (Figures 5 and 6), detailed discussion of similar bond parameters in **IIA/B** is only reported in the Supplementary Material (Par. II(b)).

However, as was found for **IA/B**, significant differences between the geometries of **IIA** and **IIB** (see also Figure S13) are clear from the expanded torsion angles O-Rh-Rh′-O′ and C6-Rh-Rh′-C6′: 89.9(6) and 176.2(6) for **IIA**, *vs* 131.2(3) and 37.7(5) for **IIB**, again justifying the configurations as *Syn-mu*-[Rh(**R**Car)Cl]$_2$ and *Anti-mu*-[Rh(**R**Car)Cl]$_2$.

3.3.3. Selected general correlation between IA/B and IIA/B

The solid–state structures of two novel dinuclear complexes; [Rh(**S**Car)Cl]$_2$ (**IA/B**) and [Rh(**R**Car)Cl]$_2$ (**IIA/B**) were studied by a single crystal X–ray diffraction study. The diolefinic ligands are enantiomers of the terpenoid carvone, a limonene derivative, and are therefore structurally similar apart from the chirality. Both **IA/B** and **IIA/B** contain two structurally different molecular entities (Figures 4 and 5), each with two rhodium(I) centers connected by two bridging chlorido ligands as well as π–bonded by the two alkene fragments of the respective diolefins, to each respective Rh center. In agreement with the IR data of **IA/B**, and **IIA/B** [44] and that of previously described rhodium(I) carvone complexes [44,46], the carbonyl group of the carvone ligand is not involved in the chelate bonding.

The two novel complexes both crystallized in the orthorhombic crystal system in the space group $P2_12_12_1$ containing eight formula units in the unit cell. Only one applicable rhodium system was identified on the CSD [43] and was used for comparison; [Rh(**S**Car)Cp] [44]. (**E**) The complex crystallized in the orthorhombic crystal system in the $P2_12_12_1$ space group with four formula units in the unit cell. Selected crystallographic data and bond parameters for **IA/B** and **IIA/B**, as well as the literature structures were given in Table 2 to identify/illustrate any similarities and/or differences.

General correlations in **IA/B** and **IIA/B** with respect to olefin [12–15,44,46–51] and chloride [52] bonding are further discussed in the Supplementary Material.

The root mean square (RMS) is the square root of the mean squared error and is used to measure the geometric difference between the packing patterns or features in crystal structures [53]. Overlaying the structures **IA/B** mu-[Rh(**S**Car)Cl]$_2$ and **IIA/B** mu-[Rh(**R**Car)Cl]$_2$ (Figure 7), by inverting the latter structure gives RMS values of 0.0180 for Rh$_A$;Rh$_B$ and 0.0175 for Rh$_C$;Rh$_D$. This indicates that there are only small differences in the relative geometry of the two crystals, ignoring the fact that they are enantiomers. It is therefore concluded that the enantiomerism described here does not, crystallographically, give rise to any significant differences.

4. Conclusion

The mu-Rh(I)-chlorido dinuclear complexes formed using the natural occurring limonene-type enantiomeric diene nucleophiles, (S)- and (R)-carvone [**S**Car and **R**car], were presented and the single crystal structures of the enantiomers reported. By utilizing the diolefinic bonds of the carvones, mu-[Rh^I(**S**Car)Cl]$_2$ (**IA/B**) and mu-[Rh^I(**R**Car)Cl]$_2$ (**IIA/B**) were obtained in ca. 80% yields in clean reactions with reactant RhCl$_3$(H$_2$O)$_x$. The "structured" chiral nanomaterials each crystallize as two independent, dinuclear molecules (based on the relative orientation of the carvone ring, oxo and methyl groups), i.e. Syn-mu-[Rh^I(**S**Car)Cl]$_2$ (**IA**), $Anti$-mu-[Rh^I(**S**Car)Cl]$_2$ (**IB**), and Syn-mu-[Rh^I(**R**Car)Cl]$_2$ (**IIA**, $Anti$-mu-[Rh^I(**R**Car)Cl]$_2$ (**IIB**), respectively. The molecules exhibit sizes larger than 1 nm (thus structured molecular nano materials), indicated by peripheral O-H8′ intra-atomic distances of 11.2(1) Å in **IA/IIA**, and 12.0(1) Å and **IB/IIB**, respectively. Important structural differences between the **IA/IIA** vs **IB/IIB** complexes in the solid state lies in the relative orientation of the two carvones, inducing a significant change in the distortion of the two intra-Rh(I) fragments in particular in the Rh$_2$Cl$_2$ core, with the dihedral angles of 49.7(1)°/49.73(6)° in **IA/IIA** (Syn-mu geometry), versus 23.8(1)°/24.00(6)° in **IB/IIB** ($Anti$-mu geometry), respectively. The presence of the two structurally independent complexes is also inferred from ^{1}H NMR spectra.

Disclosure statement

No potential conflict of interest was reported by the author(s).

Funding

References

[1]   H. Yuan, Q. Ma, L. Ye, G. Piao. *Molecules*, **21**, 559 (2016).
[2]   S. Mondal, S. Bandyopadhyay, M.K. Ghosh, S. Mukhopadhyay, S. Roy, C. Mandal. *Anticancer Agents Med. Chem.*, **12**, 49 (2012).
[3]   B.E. van Wyk. *J. Ethnopharmacol.*, **119**, 342 (2008).
[4]   S.S. Lima, G.O. de Arruda, R.D. Renovato, M.R.M. Alvarenga. *Rev. Lat. Am. Enfermagem*, **20**, 778 (2012).
[5]   O.O. Fajinmi, O. Olarewaju, J. Van Staden. In *Medicinal and Aromatic Plants of the World - Africa*, O. O. Fajinmi, O. Olarewaju, H. Najjaa (Eds), Vol. 3, pp. 61–76, Springer, Dordrecht, Netherlands (2017).
[6]   H.P. Linder. *Front. Ecol. Evol.*, **2**, 38 (2014).
[7]   P.B. Nkosi, M.N. Sibiya. *Int. J. Afr. Nurs. Sci.*, **8**, 117 (2018).
[8]   S. Lowes, E. Montero. *AEA Pap. Proc.*, **109**, 516 (2019).
[9]   A. Reid, C.B. Oosthuizen, N. Lall. *South Afr. J. Bot.*, **128**, 257 (2020).
[10]   J.H. Doughari, M.J. Bazza. *Int. J. Microbiol. Biotechnol.*, **5**, 22 (2020).
[11]   A.N.M. Mamun-Or-Rashid, M.K. Sen, M.A.H.M. Jamal, S. Nasrin. *Int. J. Biomed. Mat. Res.*, **1**, 13 (2013).
[12]   A.C. Mesa-Arango, J. Montiel-Ramos, B. Zapata, C. Durán, L. Betancur-Galvis, E. Stashenko. *Mem. Inst. Oswaldo Cruz*, **104**, 878 (2009).
[13]   CAS Reg. No. 2244-16-8. Molecule of the week archive carvone. Available online at: https://www.acs.org/molecule-of-the-week/archive/c/carvone.html (accessed 15 July 2024).
[14]   G.C. Bond. *Discuss. Faraday Soc.*, **41**, 200 (1966).
[15]   J.A. Osborn, F.H. Jardine, J.F. Young, G. Wilkinson. *J. Chem. Soc. A*, 1711 (1966).
[16]   T. Alderson, E.L. Jenner, R.V. Lindsey. *J. Am. Chem. Soc.*, **87**, 5638 (1965).
[17]   R. Cramer. *J. Am. Chem. Soc.*, **87**, 4717 (1965).
[18]   R. Cramer. *J. Am. Chem. Soc.*, **89**, 1639 (1967).
[19]   J. Chatt, R.G. Wilkins. *J. Chem. Soc.*, 2622 (1952).
[20]   N.C. Baenziger, R.C. Medrud, J.R. Doyle. *Acta Cryst.*, **18**, 237 (1965).
[21]   H.W. Quinn, J.H. Tsai. In *Advances in Inorganic Chemistry and Radiochemistry*, H.J. Eméleus, A.G. Sharpe (Eds.), Vol. 12, pp. 217–373, Academic Press, Cambridge, MA, USA (1970).
[22]   J. Chatt, L.M. Venanzi. *Nature* **177**, 852 (1956).
[23]   J. Chatt, L.M. Venanzi. *J. Chem. Soc.*, 4735 (1957).
[24]   R. Cramer. *Inorg. Chem.*, **1**, 722 (1962).
[25]   R. Cramer. *J. Am. Chem. Soc.*, **86**, 217 (1964).
[26]   J.P. Steynberg, K. Govender, P.J. Steynberg. *Production of oxygenated products*, WO 2002014248 (2002).
[27]   C. Crause, L. Bennie, L. Damoense, C.L. Dwyer, C. Grove, N. Grimmer, W.J. van Rensburg, M.M. Kirk, K.M. Mokheseng, S. Otto, P.J. Steynberg. *Dalton Trans.*, 2036 (2003).
[28]   J. Steynberg, H. Van Rensburg, J.J. Grove, S. Otto, C. Crause. *Production of oxygenated products*, WO 2003068719 A2 (2003).
[29]   C. Dwyer, A. Assumption, J. Coetzee, C. Crause, L. Damoense, M. Kirk. *Coord. Chem. Rev.*, **248**, 653 (2004).

[30] A. Polas, J.D.E.T. Wilton-Ely, A.M.Z. Slawin, D.F. Foster, P.J. Steynberg, M.J. Green, D.J. Cole-Hamilton. *Dalton Trans.*, 4669 (2003).
[31] P.N. Bungu, S. Otto. *J. Organomet. Chem.*, **692**, 3370 (2007).
[32] Bruker. *SADABS Area Detector Absorption Correction Program*, Bruker AXS, Madison, Wisconsin, USA (2016).
[33] Bruker. *SAINT Area-Detector Integration Software*, Bruker AXS, Madison, Wisconsin, USA, (2016).
[34] G.M. Sheldrick. *Acta Crystallogr. Sect. A*, **71**, 3 (2015).
[35] O.V. Dolomanov, L.J. Bourhis, R.J. Gildea, J.A.K. Howard, H. Puschmann. *J. Appl. Crystallogr.*, **42**, 339 (2009).
[36] K. Brandenburg, H. Putz. *Diamond - Crystal and Molecular Structure Visualization*, Crystal Impact, Bonn, Germany (2020).
[37] C.F. Macrae, I. Sovago, S.J. Cottrell, P.T.A. Galek, P. McCabe, E. Pidcock, M. Platings, G.P. Shields, J.S. Stevens, M. Towler, P.A. Wood. *J. Appl. Crystallogr.*, **53**, 226 (2020).
[38] L (-)-Carvone (Number 6485-40-1). Available online at: https://www.chemicalbook.com/SpectrumEN_6485-40-1_1HNMR.htm (accessed 14 August 2024).
[39] G. Giordano, R.H. Crabtree, R.M. Heintz, D. Forster, D.E. Morris. In *Inorganic Syntheses: Reagents for Transition Metal Complex and Organometallic Syntheses*, R. J. Angelici (Ed.), Vol. 28, pp. 88–90, John Wiley & Sons, Ltd (1990).
[40] M.R. Plutino, S. Otto, A. Roodt, L.I. Elding. *Inorg. Chem.*, **38**, 1233 (1999).
[41] S. Otto, A. Roodt, L.I. Elding. *Dalton Trans.*, 2519 (2003).
[42] S. Otto, A. Roodt, L.I. Elding. *Inorg. Chem. Communs.*, **9**, 764 (2006).
[43] C.R. Groom, I.J. Bruno, M.P. Lightfoot, S.C. Ward. *Acta Crystallogr. Sect. B*, **72**, 171 (2016).
[44] W. Winter, B. Koppenhöfer, V. Schurig. *J. Organomet. Chem.*, **150**, 145 (1978).
[45] T.N. Hill, A. Roodt. *Z Anorg. Allg. Chem.*, **644**, 763 (2018).
[46] V. Schurig. *J. Organomet. Chem.*, **74**, 457 (1974).
[47] R. Cramer. *J. Am. Chem. Soc.*, **89**, 4621 (1967).
[48] J.A. Ibers, R.G. Snyder. *J. Am. Chem. Soc.*, **84**, 495 (1962).
[49] M. Green, J.A.K. Howard, R.P. Hughes, S.C. Kellett, P. Woodward. *Dalton Trans.*, 2007 (1975).
[50] J.A. Ibers. *J. Organomet. Chem.*, **73**, 389 (1974).
[51] D. Allen, C.J.L. Lock, G. Turner, J. Powell. *Can. J. Chem.*, **53**, 2707 (1975).
[52] L.F. Dahl, C. Martell, D.L. Wampler. *J. Am. Chem. Soc.*, **83**, 1761 (1961).
[53] Available online at: https://www.oxfordreference.com/display/10.1093/acref/9780199233991.001.0001/acref-9780199233991-e-2676 (accessed 14 August 2024).